Mechanical Systems and Signal Processing, Volumes 66-67, January 2016, pp. 699-714
DOI:10.1016/j.ymssp.2015.05.018

Combination of Process and Vibration Data for Improved Condition Monitoring of Industrial Systems Working Under Variable Operating Conditions

C. Ruiz-Cárcel[a], V.H. Jaramillo[b], D. Mba[c], J.R. Ottewill[b], Y. Cao[a]

[a]*School of Engineering, Cranfield University, Building 52 School of Engineering, MK430AL (UK)*
[b] ABB Corporate Research Center, ul. Starowiślna 13A 31-038 Kraków, Poland
[c] *School of Engineering, London South Bank University, UK.*

Phone/ email: +44(0) 1234 754639 c.ruizcarcel@cranfield.ac.uk

Abstract

The detection and diagnosis of faults in industrial processes is a very active field of research due to the reduction in maintenance costs achieved by the implementation of process monitoring algorithms such as Principal Component Analysis, Partial Least Squares or more recently Canonical Variate Analysis (CVA). Typically the condition of rotating machinery is monitored separately using vibration analysis or other specific techniques. Conventional vibration-based condition monitoring techniques are based on the tracking of key features observed in the measured signal. Typically steady-state loading conditions are required to ensure consistency between measurements.
In this paper, a technique of merging process and vibration data is proposed with the objective of improving the detection of mechanical faults in industrial systems working under variable operating conditions. The capabilities of CVA for detection and diagnosis of faults were tested using experimental data acquired from a compressor test rig where different process faults were introduced. In addition, mechanical faults were simulated and seeded in the data to prove the validity of the proposed approach. Results suggest that the combination of process and vibration data can effectively improve the detectability of mechanical faults in systems working under variable operating conditions.

Keywords: Condition monitoring; Non-stationary operation; Compressor; Vibration; Canonical Variate Analysis

1. Introduction

The detection and diagnosis of faults in industrial systems is a very active field of research due to the reduction in maintenance costs achieved though the implementation of improved condition monitoring methods. A reduction of the number of unplanned shutdowns, improvement of system availability, capacity to pre-order spare parts as needed, increased safety in plant operations and the increase of the process efficiency are some of the main benefits of condition based maintenance. Modern industrial facilities are heavily automated and instrumented; consequently there is a lot of process data available which can be used to monitor the condition of the system. The difficulties attached to the development of accurate and reliable first-principle models of large and complex industrial facilities have led to the success of data driven methods for condition monitoring such as Principal Component Analysis (PCA), Partial Least Squares (PLS) or Canonical Variate Analysis (CVA) [1]. Literature gives examples of extensive application of these methods for detection and diagnosis of faults using computer simulated data [2-5] or real data obtained from industrial facilities or experimental test rigs [6-12]. Despite their success, PCA and PLS (and their corresponding dynamic approaches known as Dynamic PCA and Dynamic PLS [13; 14]) have been reported not to be as efficient as other state-space based methodologies such as Canonical Variate Analysis (CVA). The benefits of CVA are especially relevant when applied to systems working under variable loading conditions, principally due to the representation of the system dynamics [15-17].

Despite the success of the aforementioned methods in the detection and diagnosis of process faults, these methodologies can be insensitive to incipient mechanical faults if only process variables are analysed, as typical faults such as misalignment or unbalance have a minor effect on the performance of the machine during the early stages of degradation. However, this kind of fault can have a disastrous effect on the machines, causing catastrophic failures if the malfunction is not corrected due to the dynamic effects of the additional loads generated by the faulty condition. Vibration-based condition monitoring is probably the most common method for detection and diagnosis of mechanical faults in rotating machinery and it has several advantages against other methods. Typically, analysis of the vibration frequency spectrum can point directly to the source of the fault and there are plenty of signal processing techniques available to help the user to undertake diagnosis in conditions of high background noise.

The simplest and most used method to detect the presence of faults with vibration analysis involves a comparison of different signal features (such as RMS value, Kurtosis or peak amplitude) in the measured signal against a machine working under healthy conditions. Assuming that the initial status of the machine was healthy, any changes in the measured feature response are caused by the deterioration of the machine condition. However, this assumption is only valid if all the measurements are taken under the same loading conditions, as different levels of load will generate different vibration levels [18]. It is possible to find in literature some examples of techniques used to monitor the condition of machines working under variable loading conditions using vibration data. McFadden [19; 20] proposed a method based on band pass filtered time-domain synchronous averaging (TSA) and Hilbert transform where Kurtosis was used as an indicator of fault severity. However there are some disadvantages in this technique due to the user involvement in the election of the bandwidth for the band-pass filter [21]. Other methods are based on the examination of time-frequency maps where the instantaneous power spectrum is represented [22], but this method does not produce a single indicator of the machine condition that can be tracked in time. Parker Jr. et al. [23] proposed a method based on change detection in the bispectral domain which produced severity indicators independent of the loading conditions, but requires long computational times. The work presented by Zhan et al. [24] proposes a technique based on motion residuals, which are calculated as the difference between the TSA of a signal and the average vibration observed in the healthy state under different loading conditions. This area has gained importance in the last years and Braun [25] reviewed the state of the art of vibration diagnostics using TSA in 2011. Other methodologies presented recently are based on capturing the correlation between features extracted from the vibration signal and the operating conditions. This kind of approach has been applied successfully for diagnostics of planetary gearboxes in a bucket wheel excavator [26] and wind turbine bearing diagnostics [27].

There are several examples in industry where machines are working under severe changes in loading conditions, such as wind turbines. Industrial needs are evolving towards more flexible production schemes in order to promote efficiency and maintain their competitiveness in a market where the demand, the price of raw materials and even the price of the energy can be very volatile. That is why it is important to develop condition monitoring tools that can detect and diagnose faults in industrial systems working under variable operating conditions. These improved methods should be able to deal with both process and mechanical faults in order to ensure the quality of the product and the safe and economical operation of the plant.

In this paper we propose a method to combine process and vibration measurements in order to provide a more robust and reliable condition monitoring tool. The methodology presented here takes advantage of CVA to reveal the correlation between process and vibration measurements even under varying operating conditions in order to detect and diagnose both process and mechanical faults. The objective of the investigation is adopting signals in both time-domain such as process measurements and frequency domain such as vibration data to enhance the CVA diagnosis performance making it more sensitive to mechanical faults, which to date has not been studied in previous investigations on CVA. In order to prove the validity of the method, it was tested using experimental data acquired from a compressor test rig. The results suggest that it is possible to improve the performance of the CVA method in a real system by adding vibration data in the analysis.

2. Methodology

2.1 CVA for fault detection in industrial processes

The main objective of the most popular multivariate algorithms for process monitoring is to convert the high-dimensional data acquired from the system into a single health indicator that provides information about the condition of the process. This conversion is achieved by projecting the data using a transformation matrix, with the objective of minimizing the data variability caused by noise whilst retaining the relevant information contained within the data. Initially it is necessary to acquire data from the system working under normal operating conditions that will be used to calculate the transformation matrices and the thresholds for the health indicators. These initial data sets used to construct the algorithm are called training data sets.

The objective of CVA is to find the linear combinations that maximize the correlation between two sets of variables. This method was first developed by Hotelling in 1936 [28] and the pioneer in using this technique for system identification was Akaike in 1975 [29] using CVA between past and future data sets. This technique was later improved by Larimore [30] adapting it to general linear systems. The main advantage of CVA against other algorithms is its capacity to detect and diagnose faults in systems working under dynamic (varying) conditions. In order to take into account time correlations, at each time point k of the training period the observation vector $\boldsymbol{y_k}$ is

expanded by considering p previous and f future measurements (each one containing m variables). This operation generates the past and future observation vectors $\boldsymbol{y}_{p,k}$ and $\boldsymbol{y}_{f,k}$ respectively:

$$\boldsymbol{y}_{p,k} = \begin{bmatrix} \boldsymbol{y}_{k-1}^T & \boldsymbol{y}_{k-2}^T & \cdots & \boldsymbol{y}_{k-p}^T \end{bmatrix} \in \Re^{mp} \tag{1}$$

$$\boldsymbol{y}_{f,k} = \begin{bmatrix} \boldsymbol{y}_{k}^T & \boldsymbol{y}_{k+1}^T & \cdots & \boldsymbol{y}_{k+f-1}^T \end{bmatrix} \in \Re^{mf} \tag{2}$$

To avoid domination of those variables with higher absolute values, each variable within the data are normalized to zero mean and unit variance. The number of past and future lags (p and f) considered has a noteworthy effect on the results obtained. The optimal parameter selection can be carried out by computing the autocorrelation function of the summed squares of all measurements [17] and selecting a number of lags for which the autocorrelation is still significant. All the past and future vectors are arranged together in different columns generating the past and future matrices $\boldsymbol{Y}_p$ and $\boldsymbol{Y}_f$:

$$\boldsymbol{Y}_p = \begin{bmatrix} \hat{\boldsymbol{y}}_{p,p+1}, \hat{\boldsymbol{y}}_{p,p+2}, \ldots \hat{\boldsymbol{y}}_{p,p+M} \end{bmatrix} \in \Re^{mp \times M} \tag{3}$$

$$\boldsymbol{Y}_f = \begin{bmatrix} \hat{\boldsymbol{y}}_{f,p+1}, \hat{\boldsymbol{y}}_{f,p+2}, \ldots \hat{\boldsymbol{y}}_{f,p+M} \end{bmatrix} \in \Re^{mf \times M} \tag{4}$$

where $M=N-f-p+1$ for a data set of N observations, and $\hat{\boldsymbol{y}}_p$ and $\hat{\boldsymbol{y}}_f$ represent normalized past and future vectors respectively. The vectors $\boldsymbol{u}$ and $\boldsymbol{v}$ which solve the optimization problem of finding the linear combinations that maximize the correlation between the two data sets can be calculated by decomposing the scaled Hankel matrix using Singular Value Decomposition (SVD):

$$\boldsymbol{H} = \boldsymbol{\Sigma}_{ff}^{-1/2} \boldsymbol{\Sigma}_{fp} \boldsymbol{\Sigma}_{pp}^{-1/2} = \boldsymbol{U} \boldsymbol{D} \boldsymbol{V}^T \tag{5}$$

where $\sum_{\boldsymbol{A},\boldsymbol{B}}$ represents the sample covariance matrix of two matrices $\boldsymbol{A}$ and $\boldsymbol{B}$, and the vectors $\boldsymbol{u}$ and $\boldsymbol{v}$ are the columns of the orthogonal matrices $\boldsymbol{U}$ and $\boldsymbol{V}$ arranged in decreasing order of correlation, which is indicated by the value of the elements γ_i in the diagonal matrix $\boldsymbol{D}$. By analysing the value these elements in $\boldsymbol{D}$ ($\gamma_1 > \gamma_2 > \ldots > \gamma_{mp}$) it is possible to select the first r columns of $\boldsymbol{V}$ which best represent the correlation between $\boldsymbol{U}$ and $\boldsymbol{V}$, generating a new dimensionally reduced matrix $\boldsymbol{V}_r$. The transformation matrices $\boldsymbol{J}$ and $\boldsymbol{L}$ which convert the $m \cdot p$-dimensional past measurements to the r-dimensional canonical variates and the residuals can be calculated as:

$$\boldsymbol{J} = \boldsymbol{V}_r^T \boldsymbol{\Sigma}_{pp}^{-1/2} \qquad \boldsymbol{L} = (\boldsymbol{I} - \boldsymbol{V}_r \boldsymbol{V}_r^T) \boldsymbol{\Sigma}_{pp}^{-1/2} \tag{6, 7}$$

The canonical variates $\boldsymbol{z}_k$ and the residuals $\boldsymbol{\varepsilon}_k$ are calculated by projecting the acquired data into the low-dimensional space:

$$Z = \boldsymbol{J} \cdot \boldsymbol{Y}_p \qquad \mathbf{E} = \boldsymbol{L} \cdot \boldsymbol{Y}_p \tag{8,9}$$

where the columns of $\boldsymbol{Z}$ and $\boldsymbol{E}$ are $\boldsymbol{z}_k$ and $\boldsymbol{\varepsilon}_k$ respectively at different time points k. The statistical indicators that provide information about the condition of the system are obtained converting the available past observations into a lower dimensional data. The statistical indicators more frequently used are the Hotelling T^2 statistic and Q statistic, obtained from the canonical variates $\boldsymbol{z}$ and residuals $\boldsymbol{\varepsilon}$ respectively:

$$T_k^2 = \sum_{i=1}^{r} z_{k,i}^2 \qquad Q_k = \sum_{i=1}^{mp} \varepsilon_{k,i}^2 \tag{10,11}$$

The upper control limits (UCL) for T^2 and Q can be estimated during the training period for a given significance level α such that $P(T^2 < T^2_{UCL}(\alpha)) = \alpha$ and $P(Q < Q_{UCL}(\alpha)) = \alpha$ respectively. In the conventional CVA approach these control limits are calculated assuming that the probability density functions of the T^2 and Q statistics are Gaussian, but system nonlinearities can derive into modelling errors which are not Gaussian making this assumption invalid. Odiowei and Cao [17] developed a methodology to solve this issue by estimating the actual probability density function of the statistical indicators using Kernel Density Estimations (KDE). This method was used in this investigation for the calculation of the UCL of the T^2 and Q indicators to cope with the nonlinearities of the system studied.

For this particular investigation the event of fault detection will be considered every time any of the indicators exceed the respective UCL. This makes the monitoring performance insensitive to the number of states retained r [17]. When a fault is detected it is crucial for the system operators to be able to locate the origin of the fault in order to understand the source of the problem and react to it by planning the most appropriate maintenance action. Chiang et al. [1] suggested the use of contribution plots for this matter. The objective of the procedure is to estimate how much each one of the measured variables is contributing to the final value of the statistical indicator. In CVA it is easy to calculate the contribution c of each measured variable $\hat{y}_{k,j}$ to the final value of each of the canonical variates $z_{k,i}$ at a particular time point k:

$$c_{i,j} = \frac{z_{k,i}}{\gamma_i} J_{i,j} \cdot \hat{y}_{k,j} \tag{12}$$

where γ_i is the singular value corresponding to the loading vector $\boldsymbol{J}_i$. The total contribution C of the j_{th} process variable y_j can be obtained as:

$$C_j = \sum_{i=1}^{r} c_{i,j} \tag{13}$$

This technique has been successfully applied by other researchers for identification of process faults [31-34] representing the information in contribution plots. Once a fault has been detected, it is possible to prioritize the possible variables responsible for the fault based on their individual contributions. The plant engineers can use this information together with their plant knowledge to determine the origin of the fault.

2.2 Combination of process and vibration data for CVA application

As mentioned in section 1, most vibration-based monitoring techniques involve the observation of changes in characteristic features of the vibration signal which can point to mechanical faults. Each mechanical fault has a determined "signature" in the vibration signal that can be observed in the time or frequency domain, such as changes in the RMS or Kurtosis values, presence of peaks at particular frequencies in the signal spectrum, appearance of new peaks or sidebands, etc. These changes are used to detect the fault, locate its source, identify the type of fault and measure its severity. The evolution of these changes in the vibration signal can be tracked in time, using either continuous or intermittent observations. An example of this procedure can be found in [35], where the historic trend of vibration amplitude and phase at 1X and 2X in the frequency spectrum is monitored over time to observe the development of a flexible coupling failure.

The proposed approach consists in the extraction of the desired features from the vibration signal (or other type of signal such as current, pressure…) at the same rate as the rest of process variables are sampled. Normally vibration signals, as well as alternating current measurements, require a much higher sampling rate than conventional process measurements such as pressure, flow rate or temperature, due to the fast dynamics of vibration and current measurements. The concept represented in Fig. 1 consists of splitting the vibration signal into segments, obtaining one segment for each process measurement acquired. The length L of these segments can vary depending on the requirements (time window represented, resolution of the frequency spectrum…) and can overlap each other depending on the selected length. For every process measurement acquired at time t_i, the L samples acquired in the vibration signal immediately before t_i are extracted to configure the corresponding signal section, obtaining one section for each process measurement. Then, for each one of the sections it is possible to extract the desired features in the time domain (RMS, Kurtosis…) or in the frequency domain after windowing the corresponding section and performing a short Fourier transform (SFFT).

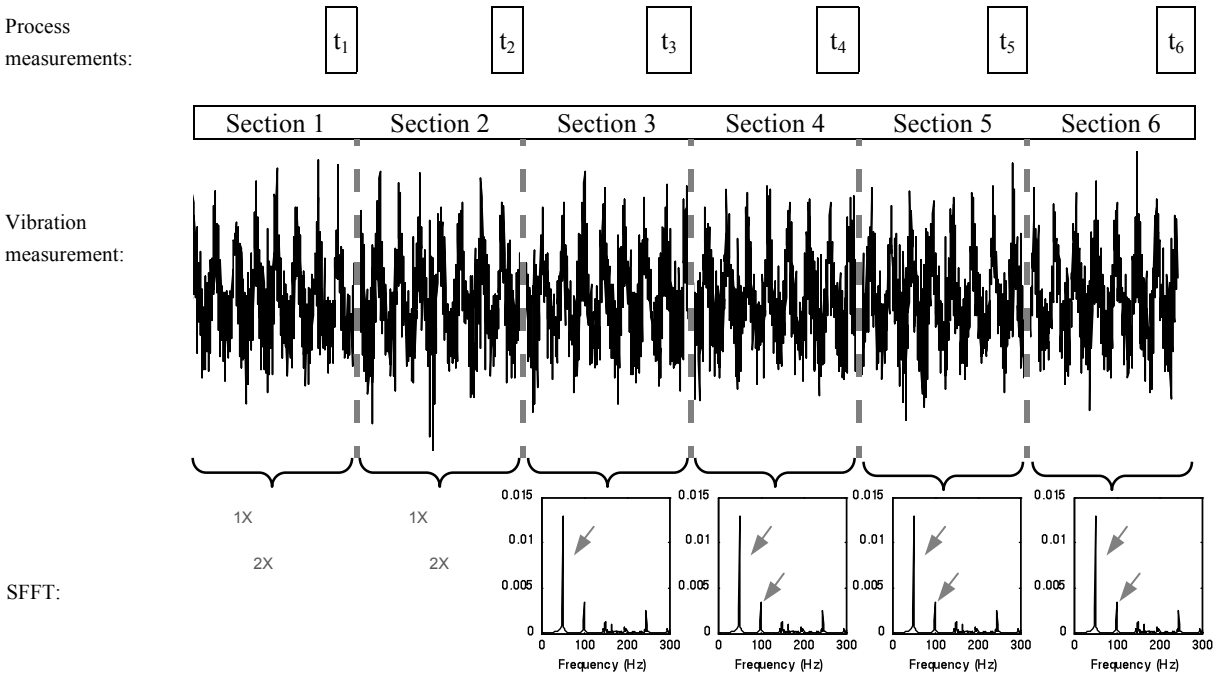

Fig. 1: Vibration signal feature extraction

Once the desired features have been extracted from the vibration signal, the values obtained can be combined with the process measurements in a single data matrix, which can be used to perform a CVA analysis (see Fig. 2):

	Process measurements				Vibration measurements		
time	Outlet pressure (bar)	Temperature (°C)	Motor speed (rpm)	Flow rate (m^3/h)	Vibration RMS (g)	1X Vibration amplitude (g)	2X Vibration amplitude (g)
t_1	1.203	12.61	1999.65	501.6	0.062	0.0131	0.0046
t_2	1.189	12.60	1999.72	502.2	0.074	0.0136	0.0041
t_3	1.926	12.63	1999.70	502.8	0.081	0.0142	0.0049
…	…	…	…	…	…	…	…
t_n	2.468	11.56	3999.12	628.3	0.126	0.0216	0.0071

Fig. 2: Example of combined data matrix containing process and vibration measurements

The use of multivariate algorithms to monitor characteristic features of vibration measurements is not new. As an example, Ahmed et al. [36] used PCA to successfully detect and diagnose faults in a reciprocal compressor extracting parameters like peak factor, RMS, entropy, crest factor, etc. from the vibration signals acquired. The methodology proposed here does not only track changes in the features extracted from vibration signals. This method takes advantage of CVA to reveal the correlation between process and vibration measurements even under varying operating conditions in order to improve the detection and diagnosis of process and mechanical faults. After the extraction of the desired features from the vibration signal the rest of the signal containing non-relevant information is dismissed, so as to minimize the amount of memory required to record the data, which is one of the main drawbacks of permanent vibration monitoring systems.

2.3 Simulation of mechanical faults in vibration data

In order to assess the performance of the proposed methodology it is necessary to obtain process and vibration data which has been acquired simultaneously from a system working under changing operational conditions in the presence of faults. The data acquisition system installed on the rig described in section 2.4 was ideal for that purpose, and several data sets were acquired from the system working under different induced process faults. However, for safety reasons it was not possible to introduce mechanical faults in the rig whilst ensuring the mechanical integrity of all its components. That is why for this analysis the vibration signature of different mechanical faults was simulated and then seeded in the acquired data. In research it is normal practice to use simulated vibration data for the study of different mechanical faults, being rotor unbalance, shaft misalignment and bearing fault the most common examples [37-45].

Rotor unbalance is caused by the displacement of the rotor center of mass away from its rotation center. The centrifugal force generated $\Delta F(t)$ has an amplitude proportional to the rotor mass m_r, the eccentricity e and the square of the rotational speed ω, and has a phase angle δ:

$$\Delta F(t) = \omega^2 m_r e \cdot \sin(\omega t + \delta) \tag{14}$$

This relation was used by Sekhar et al. [38; 45] in order to model the effect of the additional forces generated by rotor unbalance in the vibration of the system, which is basically an increase in the amplitude of the 1X peak in the frequency spectrum. The same procedure was used here to reproduce the effects of rotor unbalance.

Vibrational response due to misalignment in shafts connected by flexible couplings has been studied in several investigations [38-44]. All of them agree that the most common effect of misalignment in the vibration signal is an increase in the amplitude of the peak at 2X due to the change in the assembly stiffness twice per revolution, although 1X and other harmonics can also be affected depending on the running speed and the type of coupling. An example of the forces generated by a 1.5° angular or 1.5 mm parallel misalignment are presented in [39], where the oscillating part of the force signal has a typical peak to peak amplitude of around 100 N. The evolution of the 2X peak amplitude for an experimental case of increasing misalignment can be seen in [42].

In [37] bearing faults are simulated in a simplified manner as impacts periodically repeating at the characteristic defect frequency. An improved simulation method is proposed where the duration of the impact corresponds to the time that it takes for the rolling element to pass over the defect. The peak amplitude of the acceleration response generated is in the order of 1 m/s^2. The same approach was used in this investigation to simulate a bearing fault in the drive-end bearing of the electric motor.

Once the forces generated by the fault are known its effect on the system can be represented as a residual load $\Delta F(t)$ which acts on the undamaged system adding this new force to the already existing forces [45]. Consequently, the motion observed in the damaged system is a combination of the motion caused by the excitation forces in the undamaged system and the motion caused by the virtual damage forces. The problem can be represented in a simplified manner as a one degree of freedom system where a mass *m* is connected to the foundation by an elastic element with stiffness *K* and a viscous damper with damping *D* which during normal operation is subjected to a force $F_0(t)$. The motion $u_0(t)$ of the undamaged system can be obtained solving the equation:

$$m \cdot \ddot{u}_0(t) + D \cdot \dot{u}_0(t) + K \cdot u_0(t) = F_0(t) \tag{15}$$

When a fault affects the system the additional force $\Delta F(t)$ changes its vibrational behaviours whose motion $u(t)$ can now be obtained from:

$$m \cdot \ddot{u}\ (t) + D \cdot \dot{u}(t) + K \cdot u(t)\ \ = F_0(t) + \Delta F(t) \tag{16}$$

The residual vibrations $\Delta u(t)$ induced by the fault represent the difference between the vibrations produced in the damaged and undamaged system:

$$\Delta u(t) = u(t) - u_0(t) \tag{17}$$

Consequently the motion equation for the residual vibration generated by the fault is given by:

$$m \cdot \Delta\ddot{u}\ (t) + D \cdot \Delta\dot{u}(t) + K \cdot \Delta u(t)\ \ = \Delta F(t) \tag{18}$$

This equation was used to simulate the vibration response to unbalance, misalignment and bearing fault with the assumptions mentioned above. The solution of this equation can be obtained as the convolution of the force signal and the impulse response function $h(t)$ of the transmission path from the source to the measurement point if the force function is represented as a sequence of impacts:

$$\Delta u(t) = conv(\Delta F(t), h(t)) \tag{19}$$

The solution of this equation can be calculated more efficiently in the frequency domain, as the convolution operation turns into a simple multiplication in the frequency domain:

$$\Delta u(f) = \Delta F(f) \cdot h(f) \tag{20}$$

The impulse response function depends on the parameters *m, D* and K which define the dynamic properties of the transmission path between the source of the excitation fault (the corresponding bearing) and the measurement point. In order to simulate accurately the response generated by the fault it is important to select these parameters appropriately. Unfortunately the damping and stiffness in the motor installed in the rig used for this investigation were unknown. Its estimation via experimental tests such as the hammer test was complicated due to the difficulties related with the force application point and the fact that there is a rolling element bearing in the transmission path. However the exact estimation of vibrational response is not required in this work, as its main aim is to demonstrate that it is possible to track changes in the vibration signal due to typical mechanical faults using CVA and not to simulate these faults with perfect accuracy. For this reason, the unknown parameters were selected according to typical values used in literature [38; 45] making sure that the results obtained are coherent with the vibration measurements taken from the system.

2.4 Experimental set up

The data sets used in this investigation were acquired from a laboratory-scale compressor test rig, designed to be able to function over a wide range of operating conditions through the control of the motor rotational speed and the opening of valves situated in the compressor inlet and outlet lines.The rig is shown schematically in Fig. 3, which also includes details of the different components of the installation and some of the measured signals. The list of tags of the variables included in the analysis is indicated in Table 1.

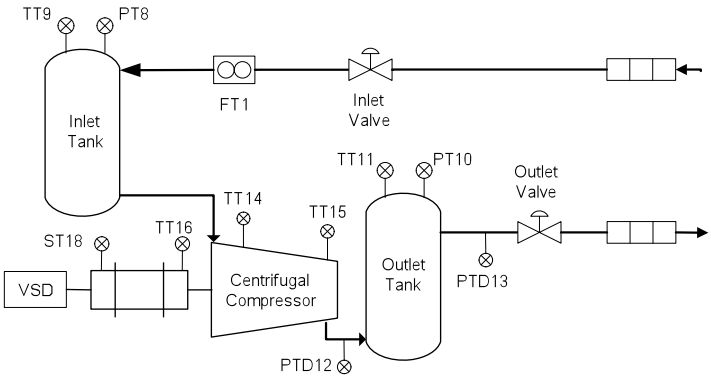

Fig. 3: Schematic representation of the gas compression experimental rig

Basically the rig is composed of a 5 stage centrifugal compressor (Continental Industrie 020.05) driven by an induction motor (ABB M3AA 160 MLB2) the speed of which can be modified using a variable speed drive (ABB ACS800) connected to the grid through a transformer. The inlet line of the compressor is composed of a 90 mm diameter PVC pipe line, a silencer, an inlet valve operated by an electric motor and a 0.5 m^3 tank. Similarly the outlet line is composed of a 90 mm diameter PVC pipe line, a 0.5 m^3 tank, a pneumatically operated valve and a silencer. Air is collected from and exhausted to the atmosphere. The motor-compressor arrangement can be seen in Fig. 4, which also shows the accelerometers installed on the motor and the compressor. Table 1 summarizes the process variables acquired during the experiments.

Fig. 4: Arrangement motor-compressor

Table 1: List of process variables

Variable nr	Location	Measured Magnitude	Units
1	Estimated	Motor torque	Nm
2	FT1	Air Flow	Sm^3/h
3	PT8	Inlet Tank Pressure	bar
4	TT16	Motor Phase Temperature	°C
5	TT9	Inlet Tank Temperature	°C
6	TT14	Left Bearing Temperature	°C
7	PDT12	Differential Pressure 1 (orifice plate)	bar
8	TT15	Right Bearing Temperature	°C
9	TT11	Outlet Tank Temperature	°C
10	Drive	Drive Current	A
11	ST18	Speed (Encoder)	rpm
12	ZT4	Outlet Valve Feedback	%
13	PT10	Outlet Tank Pressure	bar
14	PDT13	Differential Pressure 2 (orifice plate)	bar

In addition to the process variables listed in Table 1, 6 accelerometers and 3 current sensors were installed on the rig to monitor the vibration levels and motor current during the experiments. On the motor the accelerometers were placed in the horizontal and vertical direction on the drive end of the motor casing, in addition to a third accelerometer placed on one of the motor feet. On the compressor 2 accelerometers were placed on the casing of the drive end bearing (vertical and horizontal) and a third one was placed in the axial direction on the non-drive end. The accelerometers used were SKF CMSS2110 (frequency range 0.8Hz-10kHz) in all cases except on the motor foot, where the model IMI 608A11 (frequency range 0.5Hz-10kHz) was selected due to its smaller size. The vibration data was acquired at a sampling rate of 5120Hz using a NI 9234 data acquisition card which included an antialiasing filter. The current drawn by the motor was measured in each one of the phases using an ABB EL55P2 sensor. The current signal was acquired at a sampling rate of 5kHz using a NI9203 data acquisition card. The measurements of vibration and current were synchronised with process measurements by the use of the timestamps produced by the data acquisition system, making sure that the start and end time for all the data sets was exactly the same in each experiment.

2.5 Acquisition of data sets

During the various experiments conducted, the process variables listed in Table 1 were originally sampled at 1 kHz. In this investigation the acquired process variable data sets were down sampled to 1 Hz, which is more in line with sampling rates typically seen in industry. During the tests, the motor speed and the position of the outlet valve were given different control set points in order to obtain data from the system working under variable operating conditions. Throughout testing the inlet valve was set to be fully open. As well as reducing the number of potential operating points to be considered as normal operation, this approach allowed the valve to be used to simulate a blockage in the inlet pipeline.

In addition to the process variables listed in Table 1, 15 additional variables extracted from the current, vibration and pressure sensors were included in the analysis following the methodology presented in section 2.2. In order to avoid redundant information and reduce computation time, the vibration signals measured in the horizontal direction were rejected for the CVA analysis of the data. Similarly only one of the three current measurements was included due to the similarities found in the signals in all three phases. The features extracted from the vibration, current and pressure signals were selected to give the CVA method a high sensitivity to typical faults such as unbalance, misalignment or compressor surge. The features selected for the CVA analysis were:

-The amplitude of the peaks at the rotational speed (1X) and its second harmonic (2X) in the spectrum of current signal, vertical vibration measured in the compressor, vertical vibration measured in the motor casing and vertical vibration measured in the motor foot.

-RMS value of the current signal, vertical vibration measured in the compressor, vertical vibration measured in the motor casing and vertical vibration measured in the motor foot.

-Amplitude of the peak at 2.4Hz (Surge frequency) and its second harmonic (4.8Hz) in Differential Pressure 1 signal (PDT12) and amplitude of the peak at 2.4Hz in the outlet tank pressure signal (PT10). Obviously these features were extracted from the original signals acquired at 1 kHz before the data was down sampled.

In order to obtain a reasonable resolution in the frequency spectrum of all the signals studied, the length L of the window analysed was 1s for current and vibration measurements and 5 seconds for pressure and differential pressure measurements. Table 2 summarizes the variables constructed by the extraction of these characteristic features in the time and frequency domain which were included in the CVA analysis:

Table 2: List of process variables

Variable nr	Origin	Measured Magnitude	Units
15	Current	Amplitude of peak at 1X	A
16	Current	Amplitude of peak at 2X	A
17	Current	RMS	A
18	Compressor vibration	Amplitude of peak at 1X	g
19	Compressor vibration	Amplitude of peak at 2X	g
20	Compressor vibration	RMS	g
21	Motor casing vibration	Amplitude of peak at 1X	g
22	Motor casing vibration	Amplitude of peak at 2X	g
23	Motor casing vibration	RMS	g
24	Motor foot vibration	Amplitude of peak at 1X	g
25	Motor foot vibration	Amplitude of peak at 2X	g
26	Motor foot vibration	RMS	g
27	Differential pressure1 (DPT12)	Amplitude of peak at 2.4Hz	bar
28	Differential pressure1 (DPT12)	Amplitude of peak at 4.8Hz	bar
29	Outlet tank pressure (PT10)	Amplitude of peak at 2.4Hz	bar

Three data sets (T1, T2 and T3) were acquired from the system working under normal operating conditions for training purposes. The operating points were selected to cover a wide range of operating conditions within the safe operating region in the compressor map, trying to avoid the surge and choke regions. In each training data set, the operational conditions were changed, though not identically, in order to obtain a good variety of large, small, long and slow process changes happening in different directions (increment or decrement). The objective of this variety in the operational conditions is to ensure that the dynamics of the system are captured in all circumstances. As an example, Fig. 5 represents the set points for the operating conditions tested in data set T1.

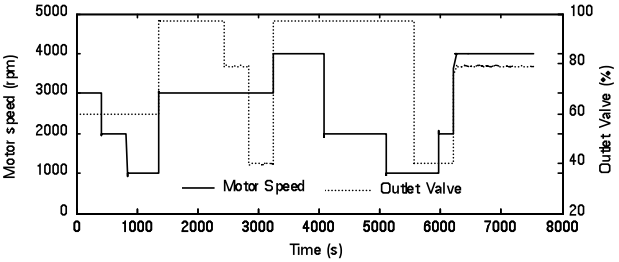

Fig. 5: Operating conditions for T1

An additional data set was acquired from the rig to study the effects of compressor surge. This phenomenon is described as the complete disruption of the air compression and reversal of the air flow inside the compressor, caused by the inability of the machine to work against the already compressed air when the pressure ratio is too high. After this disruption, the compressor will reach stable flow once the pressure ratio is reduced to a normal level and, if the operating conditions that caused the surge remain, the cycle will restart producing a new flow reversal. The appearance of this phenomenon can be critical as it can cause catastrophic damage in a compressor, but this particular rig is designed to be able to cope with surge conditions for a certain amount of time. In this data set, the compressor set point was moved to the surge region twice using different combinations of motor speed and outlet valve position.

This case was first studied analysing the 30 variables described in Table 1 and Table 2. Then this case was also studied from the vibration point of view by removing the variables related with pressure measurements from the analysis. This allowed the detection of the fault to be based on vibration measurements in order to prove the validity of the proposed method using real (not simulated) vibration data. In addition to this process fault, 3 mechanical faults were simulated following the procedure proposed in 2.3, including unbalance, misalignment and bearing fault.

3. Results and discussion

The first step for the application of CVA for monitoring purposes is the calculation of the transformation matrices and the threshold for the T^2 and Q indicators using data acquired under normal operating conditions. The optimal number of past and future lags considered in the analysis (p and f) can be calculated computing the autocorrelation function of the summed squares of all measurements [17]. The objective of this analysis is to take into consideration a number of lags which contains relevant information in terms of autocorrelation. Fig. 6 shows an example of the autocorrelation function for the training data set T1 against a confidence bound of ±5% (dashed lines).

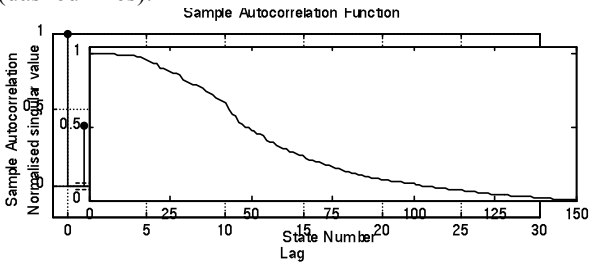

Fig. 6: Sample autocorrelation function against ±5% confidence bound (dashed lines).

Fig. 7: Normalized singular values for T1

For this study p and f were set to 5 according to the results obtained from the analysis of the autocorrelation function of the three training data sets. The most common methodologies used for the calculation of the optimal number of states retained r are the analysis of the dominant singular values in the matrix $\boldsymbol{D}$ [46] and methodologies based on the Akaike Information Criterion (AIC) [1]. Fig. 7 shows an example of normalized singular values obtained from (12) applying CVA to the training data set T1. In this particular case, setting the number of retained states based on the dominant singular values will result in an unrealistic high order model because the singular values decrease slowly [17]. In addition, the number of states retained is not especially relevant for this study because both statistical indicators (T^2 and Q) are used simultaneously for fault detection. As a result, the system variations not captured in the retained space (represented by T^2) will be captured by the residual space (Q) and vice versa.

It is essential for the analysis to use a training set that covers the entire spectrum of possible operational conditions. It is possible to combine different training data sets to enrich the variety of the data included in the analysis. In this investigation the combination was done by calculating the past and future matrices individually for each training data set according to (5) and (6) and then merging the matrices obtained. The three data sets were mixed in pairs generating 3 different combined sets that were used to check its capacity to represent the system dynamics accurately producing a low number of false alarms. CVA was performed for each one of the three combined training data sets using a range of values for the number of states retained *r* in order to select the value for this parameter that minimizes the number of false alarms produced (see Fig. 8).

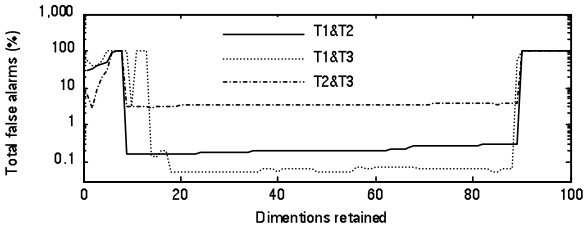

Fig. 8: Analysis of the influence of the number of states retained

The data set combination which produced lower false alarm rates was T1 and T3. The number of states retained was set to 30 (r=30) for the data analyses in order to minimize the false alarm rate in normal conditions (see Fig. 8). The UCL calculated using KDE for this configuration using 99% confidence bound was 5481.42 and 7038.46 for the T^2 and Q indicators respectively.

3.1 Compressor surge

Compressor surge was introduced by moving the compressor operating point to regimes where surge is expected. Fig. 9 represents the operating conditions (motor speed and outlet valve position) during the test (left), and the effect of the fault in the measured outlet pressure (right). The operating conditions for which surge is expected are shaded in grey.

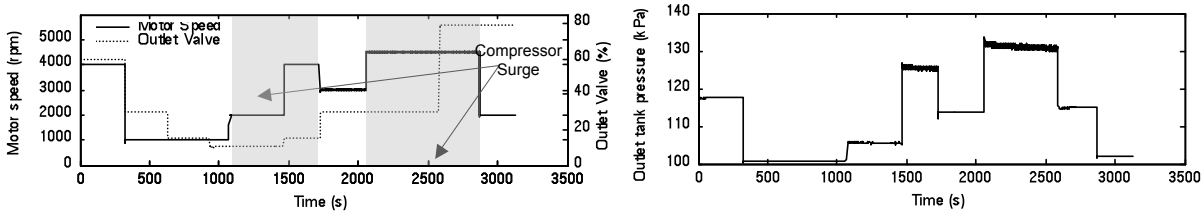

Fig. 9: Operational conditions (left) and fault evolution (right) for surge

The test duration was 3131 seconds. The surge conditions were introduced from sample 1071 to 1725 and 2062 to 2868. Normal operation is expected for the rest of samples in the test. It can be seen in Fig. 9 (right) how the faulty condition introduced caused oscillations in the outlet tank pressure. Fig. 10 represents the results obtained in terms of fault detection (left) and diagnosis (right).

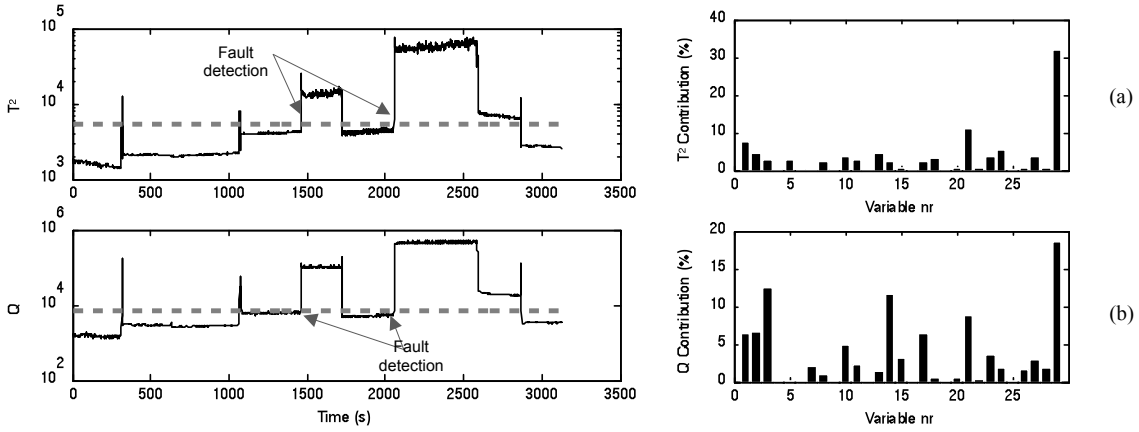

Fig. 10: Results for surge: T^2 (a) and Q (b) indicators (left) and contribution plot at sample 1459(right)

For this data set the first fault detection happened at sample 1459 for both indicators after two short false alarms which corresponded to step changes in the motor speed. The surge conditions induced from sample 1071 to 1457 were not detected by the algorithm, although the value of both indicators is high for that region. The reason for the lack of detection in that region is attributed to the low severity of surge for that particular conditions (2000 rpm and 10% valve opening), but the fault was detected almost immediately as surge was introduced at higher rotational speeds. Both indicators fall below the UCL when the fault is removed. The contribution plots at the first fault detection time (sample 1459) are represented in Fig. 10(b). The variable contributing most to the final value of both indicators is the amplitude of the peak at 2.4Hz in the frequency spectrum of the outlet tank pressure signal (variable 29). This evidences the fact that the fault is effectively caused by compressor surge and reveals the importance of being able to track features in the frequency spectrum to increase the sensibility of CVA to certain types of faults. Other significant variables contributing to the indicators are amplitude of the 1X peak in the motor vibration (variable 21), and the torque, air flow rate, inlet pressure, differential pressure 2 and current RMS value in the case of Q indicator (variables 1,2,3,14 and 17).

This result shows that variables related with features in the pressure signal spectrum and pressure measurements themselves are the most significant variables in terms of fault diagnosis (Fig. 10 (right)). Nevertheless, if those variables are removed from the analysis as well as variables related with features in the vibration and current signal spectrum, the fault was not detected by CVA with only the remaining variables. Fig. 11 represents the results obtained from CVA analysing the same surge data set but including only variables 1,2,4,5,6,8,9,10,11 and 12 (related with measurements of torque, flow rate, temperatures, current, speed and valve position) in the analysis:

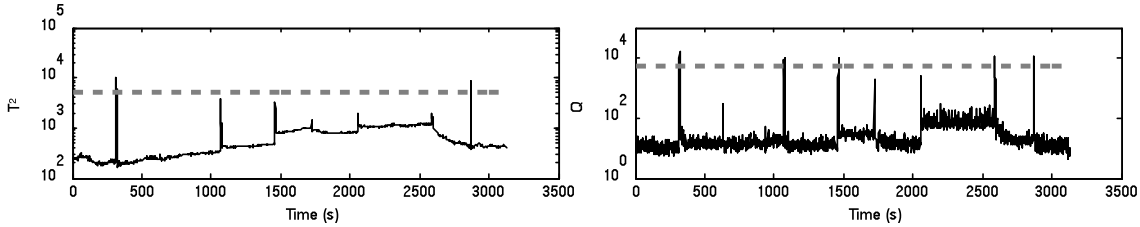

Fig. 11: T^2 and Q indicators for surge detection with limited variables

In this case the fault is invisible for the algorithm for all operating conditions. However, if the variables related with current and vibration features are added to the analysis (variables 15 to 26) the results obtained in terms of fault detection and diagnosis are very different (see Fig. 12). In terms of fault detection, the results are not as good as in Fig. 10(left) but the addition of vibration data allowed the detection of the fault, demonstrating the validity of the method using real (not simulated) vibration data. The fault was detected only by the T^2 statistic in the second introduction of surge at sample 2174 after some false alarms. The contribution plots at sample 2174 reveal the importance of the vibration features in the analysis, the amplitude of the 1X peak and the RMS value of the compressor signal being the most significant variables.

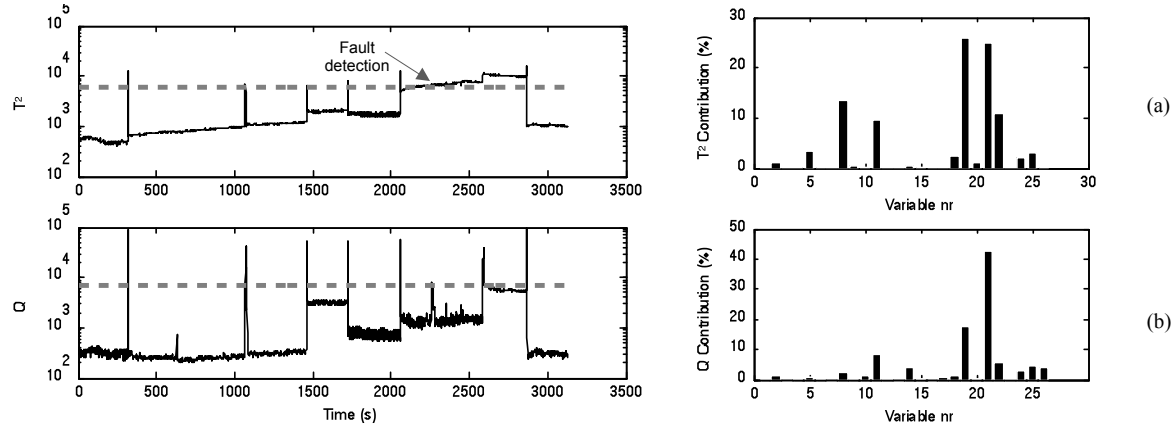

Fig. 12: Results for bearing fault: T^2 (a) and Q (b) indicators (left) and contribution plot at sample 2174(right)

3.2 Mechanical faults

The vibrational signature of 3 typical mechanical faults (unbalance, misalignment and bearing fault) was simulated using the procedures introduced in section 2.3. The acceleration signal obtained from the fault

simulation was added to the vibration signal of a specific data set acquired from the rig under normal operating conditions. The operating points selected during the test are represented in Fig. 13.

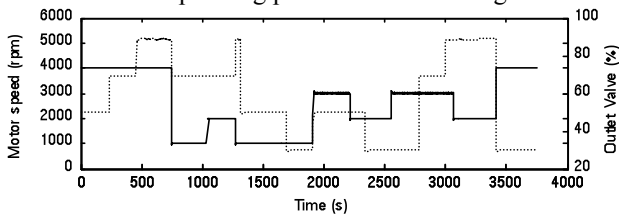

Fig. 13: Operating conditions for simulation of mechanical faults

For the simulation the vibrations due to a mechanical fault were modelled as a one degree of freedom system where a mass *m* is connected to the foundation by an elastic element with stiffness *K* and a viscous damper with damping *D*. The mass *m* represents the mass of the electric motor or the compressor (depending for which element the vibrations are being simulated) and its value is 105kg and 140kg respectively. The parameters *K* and *D* are difficult to obtain unless a specific study is carried out. For this investigation the value of these parameters was tuned used typical values based on informed literature [38; 45]. The selected values for *K* and *D* were 10^8 N/m and 1000 Ns/m respectively.

3.2.1 Rotor unbalance

The objective of this test is to simulate the vibrational response generated by rotor unbalance in the motor where the eccentricity grows linearly from perfect condition to a maximum of 0.5 mm. The residual force $\Delta F(t)$ generated by the simulated fault was estimated using (24). The obtained system response in terms of acceleration was added to the vibration measurement taken from the motor in the vertical direction and then processed for CVA analysis. The parameters used for the simulation are represented in Table 3:

Table 3: Parameters for simulation of rotor unbalance

Parameter	Value
K	10^8 N/m
C	1000 Ns/m
m	105 Kg
m_r	25 Kg
e	0-0.5 mm

Fig. 14 represents the original vibration signal measured from the motor in vertical direction Fig. 14 (left) and the combined signal after adding the simulated fault Fig. 14 (right):

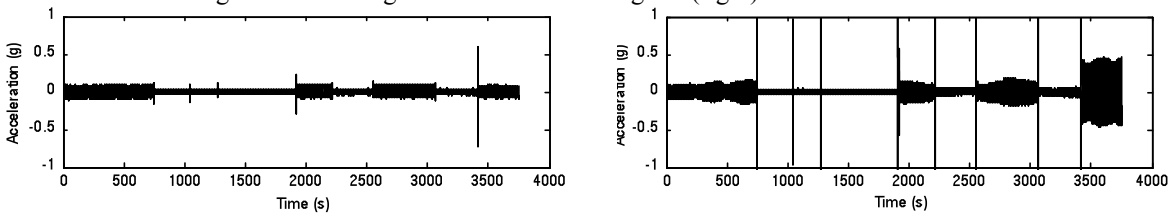

Fig. 14: Original motor vibration signal (left) and signal including seeded fault (right)

The effect of the seeded fault in the frequency spectrum of the vibration signal in the last stages of degradation (maximum unbalance) can be seen in Fig. 15.

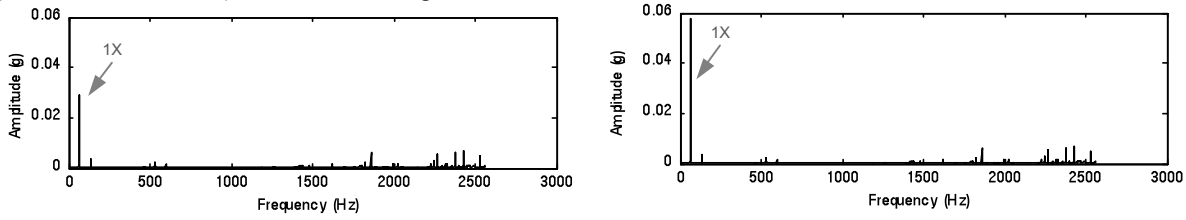

Fig. 15: Spectrum of the vibration signal before (left) and after (right) the introduction of unbalance

Fig. 16 represents the results obtained in terms of fault detection (left) and diagnosis (right) after the application of CVA to the data set:

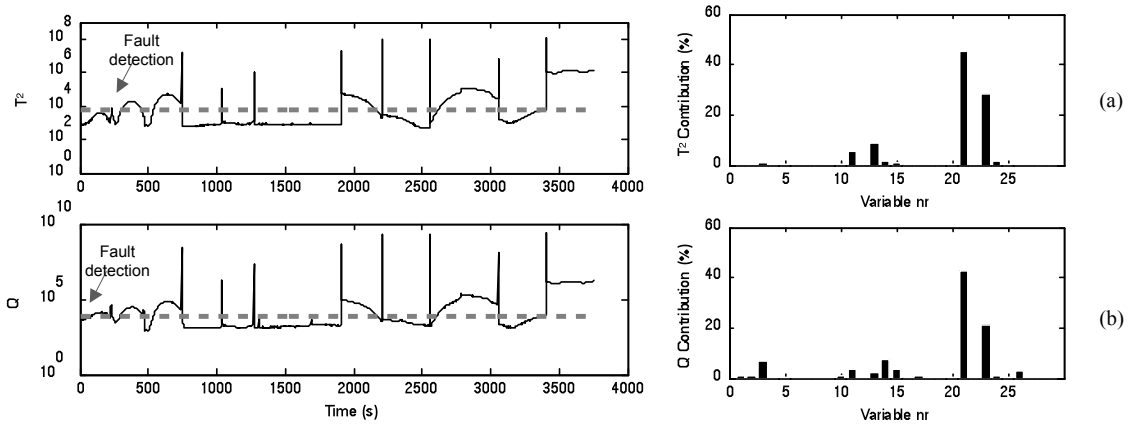

Fig. 16: Results for unbalance: T^2 (a) and Q (b) indicators (left) and contribution plot at sample 75(right)

For this data set the first fault detection happened at sample 305 for the T^2 statistical indicator after one short false alarm and at sample 75 for the Q indicator. These samples correspond to an eccentricity of 0.04mm and 0.01mm respectively. The value of both indicators fluctuates above and below the UCL depending on the operational conditions. The cause of this is the dependency of the fault severity with the motor speed. The curved shape of both indicators is attributed to differences in phase between the simulated vibration and the main component at 1X in the real vibration, caused by slight variations in the real rotating speed. This change in phase causes an effect of increase or attenuation of the vibration depending on whether or not the signals are in phase. This oscillation can also be observed in Fig. 14 (right). The variables contributing more to the final value of both indicators are the amplitude of the peak at 1X in the frequency spectrum of the vibration signal measured in the motor and the RMS value of the same signal, which shows the sensitivity of the method to changes in the vibration frequency spectrum.

3.2.2 Shaft misalignment

The objective of this test is to simulate the vibrational response generated by misalignment between the compressor and motor shafts. The residual force $\Delta F(t)$ was simplified for the analysis as a sinusoidal force with an oscillating frequency of twice the rotating speed (2X). The amplitude of the sinusoidal force grew linearly during the test from 0 to 100N at the end of the experiment simulating a linear increment in the misalignment. This approach neglects the dependence of the force generated by misalignment with the load but covers a wide spectrum of misalignment forces. The obtained system response in terms of acceleration was simulated for these loading conditions in the motor and the compressor, and added to the corresponding vibration measurement to be processed using CVA analysis. The parameters used for the simulation are represented in Table 4:

Table 4: Parameters for simulation of misalignment

Parameter	Value
K	10^8 N/m
C	1000 Ns/m
m (motor)	105 Kg
m (compressor)	140Kg
ΔF	0-100N

Fig. 17 represents the generated system response in the motor Fig. 17 (left) and the compressor Fig. 17 (right). It can be observed that there are transients of very high amplitude corresponding to motor speed step changes.

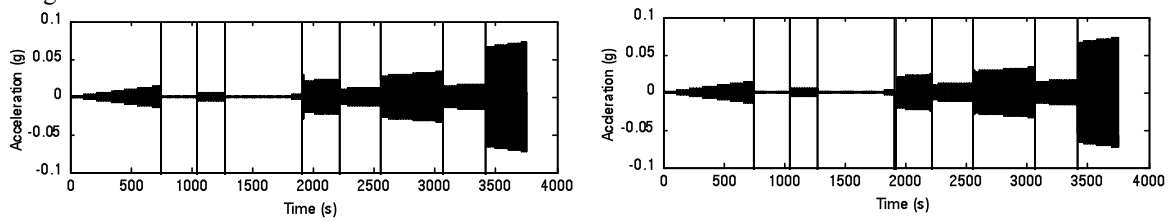

Fig. 17: System response to misalignment in motor (left) and compressor (right)

Fig. 18 represents the original vibration signal spectrum measured from the motor in vertical direction at the end of the test Fig. 18 (left) and the spectrum of the combined signal after adding the simulated fault Fig. 18 (right). It is noticeable the increase in the amplitude of the 2X peak:

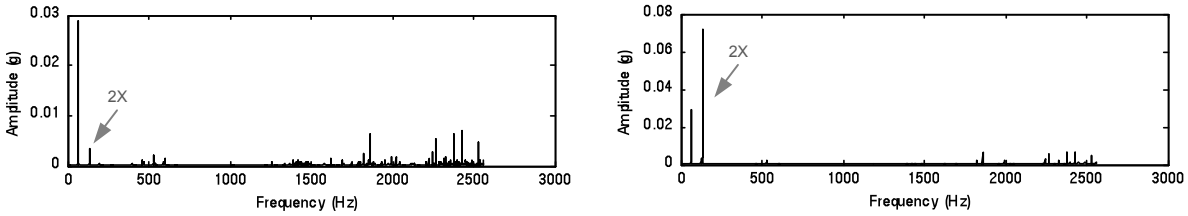

Fig. 18: Vibration frequency spectrum observed in the motor before (left) and after seeding the simulated fault (right)

Fig. 19 represents the results obtained in terms of fault detection (left) and diagnosis (right) after the application of CVA to the data set. For this data set the first fault detection occurred at sample 1908 for both statistical indicators after three and five short false alarms respectively. This sample corresponds to a force amplitude of 50.48N. After the detection point the value of both indicators fluctuates above and below the UCL depending on the operational conditions. This is due to the dependency of the fault severity with the motor speed, as can be seen in the shape of the simulated residual load in Fig. 17. Again there are oscillations in the indicators caused by the difference in phase between the simulated signal and the original component at 2X, but in this case the differences are reduced due to the low amplitude of the original 2X peak. The variables contributing more to the final value of the T^2 are the amplitude of the peak at 2X in the frequency spectrum of the vibration signal measured in the compressor (variable 19) and the motor (variable 22), the peak amplitude at 1X for both signals (variables 18 and 21), the RMS of the motor vibration signal (variable 23) and the outlet tank pressure (variable 14). In the case of the Q indicator the same variables show a high level of significance but with a different rank.

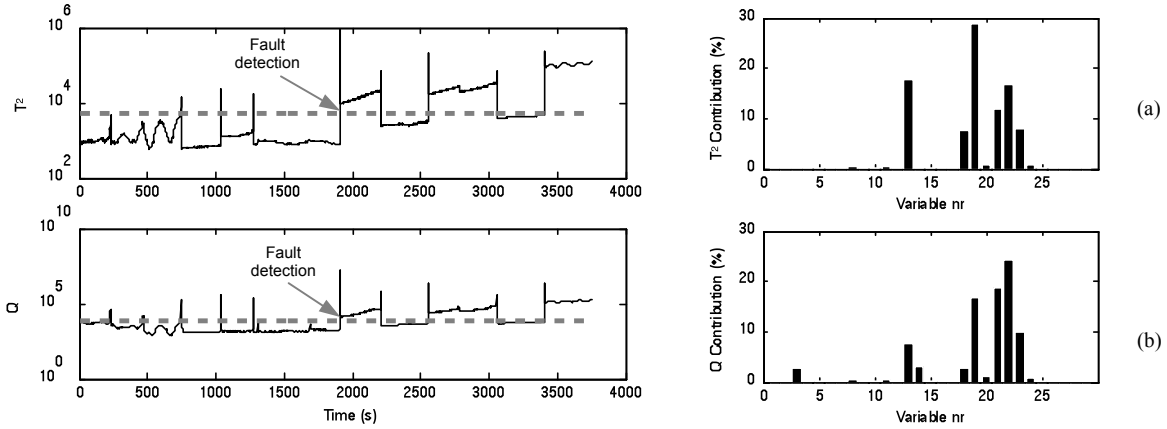

Fig. 19: Results for misalignment: T^2 (a) and Q (b) indicators (left) and contribution plot at sample 1908(right)

3.2.3 Bearing fault

The objective of this test is to simulate the vibrational response generated by an outer race bearing fault in the driven end of the motor. The fault was simulated as a series of impulses acting on the virtual system, following a similar approach as [37]. The obtained system response in terms of acceleration was added to the vibration measurement taken from the motor in the vertical direction and then processed for CVA analysis. The main bearing characteristics and the parameters used for the simulation are represented in Table 5 and Table 6:

Table 5: Main bearing characteristics

Manufacturer/model	SKF 6309-2Z
Inner diameter	45 mm
Outer diameter	100 mm
Pitch diameter	72.492 mm
Ball diameter	17.462 mm
Number of rolling elements	8
Contact angle	0°
Outer race defect frequency	3.036X
Cage rotating frequency	0.38X

Table 6: Parameters for simulation of bearing outer race defect

Parameter	Value
K	10^8 N/m
C	1000 Ns/m
m	105 Kg
Impulse frequency	3.036X
Impulse duration	0.000115s-0.0023s
Impulse amplitude	0-10N

The impulse frequency was set to 3.036X in order to simulate a fault in the outer ring. The impact duration grew linearly during the test from 0.1157 ms at the beginning and 2.3 ms at the end, which corresponds to a defect size between 0.5 mm and 10 mm if the rotor speed is 3000rpm. Fig. 20 represents the combined vibration signal observed in the motor vibration in vertical direction after adding the simulated fault (left) and the frequency spectrum of the vibration signal in the last stages of degradation (right):

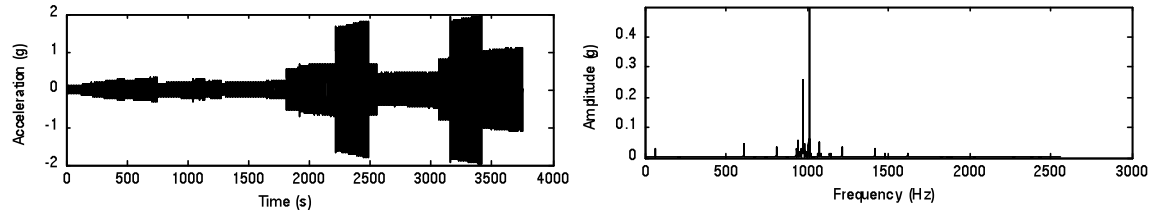

Fig. 20: System response to bearing fault in the time (left) and frequency (right) domains.

The most significant changes observed in the frequency spectrum after seeding the simulated fault are the activity increment around the virtual system natural frequency (975Hz) due to the resonant response to the impacts and the appearance of a new peak at 3.036X. Fig. 21 represents the results obtained in terms of fault detection (left) and diagnosis (right) after the application of CVA to the data set. For this data set the first fault detection happened at sample 164 for the T^2 statistical indicator and at sample 78 for the Q indicator. These samples correspond to an impact duration of 0.211ms and 0.1611ms, and an impact amplitude of 0.43N and 0.2N. The variable contributing most to the final value of both indicators is the RMS value of the motor vibration signal (variable 23).

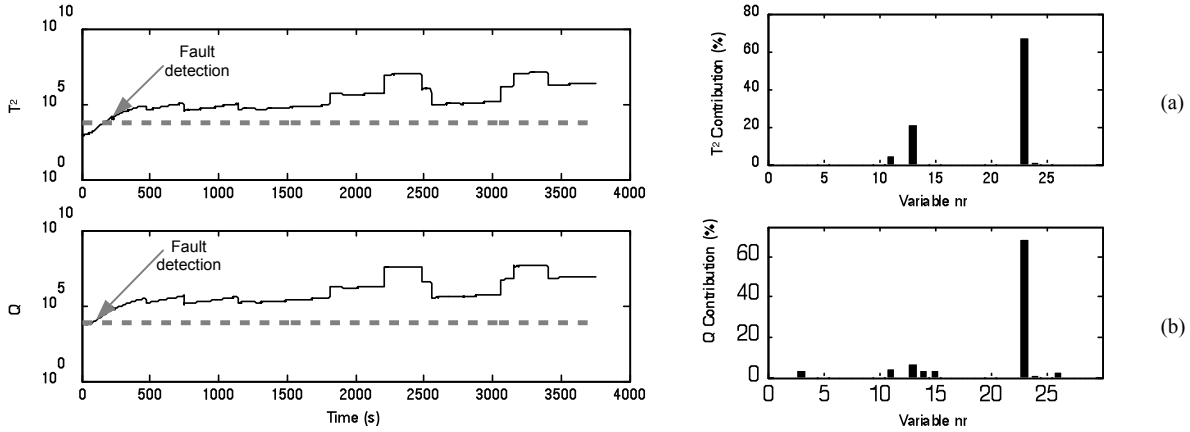

Fig. 21: Results for bearing fault: T^2 (a) and Q (b) indicators (left) and contribution plot at sample 78(right)

4. Conclusion

This paper proposes a simple method to merge process data and vibration features to improve the detectability of mechanical faults in systems working under varying operational conditions. The proposed method was tested using experimental data acquired from a compressor test rig where data sets were acquired from the system working under faulty conditions and varying operational points. Additionally mechanical faults were numerically simulated and added to vibration measurements.

The results show how CVA is able to detect changes in vibration features during the test, and detect deviations from normal operation even under operational conditions that were not considered in the training period. In addition contribution plots obtained at the time of fault detection provided valuable information about the variables most affected by the fault, which can help in root cause analysis. The analyses were carried out in a fast and robust manner, as the CVA is a well-known efficient and effective method and the proposed approach just requires the computation of short Fourier transforms and extraction of the desired features.

Acknowledgements

Financial support from the Marie Curie FP7-ITN project "Energy savings from smart operation of electrical, process and mechanical equipment– ENERGY-SMARTOPS", Contract No: PITN-GA-2010-264940 is gratefully acknowledged.

References

[1] L.H. Chiang and E.L. Rusell and R.D. Braatz (2000), *Fault detection and diagnosis in industrial systems,* 1st ed, Springer, London UK.

[2] Juricek, B. C., Seborg, D. E. and Larimore, W. E. (2004), "Fault Detection Using Canonical Variate Analysis", *Industrial and Engineering Chemistry Research,* vol. 43, no. 2, pp. 458-474.

[3] Simoglou, A., Martin, E. B. and Morris, A. J. (2002), "Statistical performance monitoring of dynamic multivariate processes using state space modelling", *Computers and Chemical Engineering,* vol. 26, no. 6, pp. 909-920.

[4] Yunus, M. Y. M. and Zhang, J. (2010), "Multivariate process monitoring using classical multidimensional scaling and procrustes analysis", *IFAC Proceedings Volumes (IFAC-PapersOnline),* Vol. 9, pp. 165.

[5] Zhou, K. -., Li, Q. -. and Guo, R. -. (2012), "Improving monitoring accuracy of process based on SPC method", *Proceedings of the 2012 24th Chinese Control and Decision Conference, CCDC 2012,* pp. 1488.

[6] Alkaya, A. and Eker, İ (2011), "Variance sensitive adaptive threshold-based PCA method for fault detection with experimental application", *ISA transactions,* vol. 50, no. 2, pp. 287-302.

[7] Borsje, H. J. (1999), "Fault detection in boilers using canonical variate analysis", *Proceedings of the American Control Conference, 1999,* Vol. 2, pp. 1167.

[8] Eserin, P. (1999), "Application of canonical variate analysis to the dynamical modeling and control of drum level in an industrial boiler", *Proceedings of the American Control Conference, 1999,* Vol. 2, pp. 1163.

[9] Lee, H. W., Lee, M. W. and Park, J. M. (2009), "Multi-scale extension of PLS algorithm for advanced on-line process monitoring", *Chemometrics and Intelligent Laboratory Systems,* vol. 98, no. 2, pp. 201-212.

[10] Peng, K. -., Li, G. and Zhang, K. (2012), "Strip thickness monitoring in hot strip mill processes based on dynamic total projection to latent structures (T-PLS) algorithm", *Kongzhi Lilun Yu Yingyong/Control Theory and Applications,* vol. 29, no. 11, pp. 1446-1451.

[11] Vanhatalo, E. (2010), "Multivariate process monitoring of an experimental blast furnace", *Quality and Reliability Engineering International,* vol. 26, no. 5, pp. 495-508.

[12] Rotem, Y., Wachs, A. and Lewin, D. R. (2000), "Ethylene compressor monitoring using model-based PCA", *AIChE Journal,* vol. 46, no. 9, pp. 1825-1836.

[13] Komulainen, T., Sourander, M. and Jämsä-Jounela, S. -. (2004), "An online application of dynamic PLS to a dearomatization process", *Computers and Chemical Engineering,* vol. 28, no. 12, pp. 2611-2619.

[14] Ku, W., Storer, R. H. and Georgakis, C. (1995), "Disturbance detection and isolation by dynamic principal component analysis", *Chemometrics and Intelligent Laboratory Systems,* vol. 30, no. 1, pp. 179-196.

[15] Juricek, B. C., Seborg, D. E. and Larimore, W. E. (2004), "Fault Detection Using Canonical Variate Analysis", *Industrial and Engineering Chemistry Research,* vol. 43, no. 2, pp. 458-474.

[16] Russell, E. L., Chiang, L. H. and Braatz, R. D. (2000), "Fault detection in industrial processes using canonical variate analysis and dynamic principal component analysis", *Chemometrics and Intelligent Laboratory Systems,* vol. 51, no. 1, pp. 81-93.

[17] Odiowei, P. -. P. and Cao, Y. (2009), "Nonlinear dynamic process monitoring using canonical variate analysis and kernel density estimations", *Computer Aided Chemical Engineering,* vol. 27, no. C, pp. 1557-1562.

[18] Stander, C. J., Heyns, P. S. and Schoombie, W. (2002), "Using vibration monitoring for local fault detection on gears operating under fluctuating load conditions", *Mechanical Systems and Signal Processing,* vol. 16, no. 6, pp. 1005-1024.

[19] McFadden, P. D. (1986), "Detecting fatigue cracks in gears by amplitude and phase demodulation of the meshing vibration", *Journal of vibration, acoustics, stress, and reliability in design,* vol. 108, no. 2, pp. 165-170.

[20] McFadden, P. D. (1988), "Determining the location of a fatigue crack in a gear from the phase of the change in the meshing vibration", *Mechanical Systems and Signal Processing,* vol. 2, no. 4, pp. 403-409.

[21] Dalpiaz, G., Rivola, A. and Rubini, R. (2000), "Effectiveness and sensitivity of vibration processing techniques for local fault detection in gears", *Mechanical Systems and Signal Processing,* vol. 14, no. 3, pp. 387-412.

[22] Baydar, N. and Ball, A. (2001), "A comparative study of acoustic and vibration signals in detection of gear failures using Wigner-Ville distribution", *Mechanical Systems and Signal Processing,* vol. 15, no. 6, pp. 1091-1107.

[23] Parker Jr., B. E., Ware, H. A., Wipf, D. P., Tompkins, W. R., Clark, B. R., Larson, E. C. and Poor, H. V. (2000), "Fault diagnostics using statistical change detection in the bispectral domain", *Mechanical Systems and Signal Processing,* vol. 14, no. 4, pp. 561-570.

[24] Zhan, Y., Makis, V. and Jardine, A. K. S. (2006), "Adaptive state detection of gearboxes under varying load conditions based on parametric modelling", *Mechanical Systems and Signal Processing,* vol. 20, no. 1, pp. 188-221.

[25] Braun, S. (2011), "The synchronous (time domain) average revisited", *Mechanical Systems and Signal Processing,* vol. 25, no. 4, pp. 1087-1102.

[26] Bartelmus, W. and Zimroz, R. (2009), "A new feature for monitoring the condition of gearboxes in non-stationary operating conditions", *Mechanical Systems and Signal Processing,* vol. 23, no. 5, pp. 1528-1534.

[27] Zimroz, R., Bartelmus, W., Barszcz, T. and Urbanek, J. (2014), "Diagnostics of bearings in presence of strong operating conditions non-stationarity—A procedure of load-dependent features processing with application to wind turbine bearings", *Mechanical Systems and Signal Processing,* vol. 46, no. 1, pp. 16-27.

[28] Hotelling, H. (1936), "Relations between two sets of variates", *Biometrika,* vol. 28, no. 3-4, pp. 321-377.

[29] Akaike, H. (1975), "Markovian representation of stochastic processes by canonical variables.", *SIAM J Control,* vol. 13, no. 1, pp. 162-173.

[30] Larimore, W. E. (1983), "System identification, reduced-order filtering and modeling via canonical variate analysis.", *Proceedings of the American Control Conference,* Vol. 2, pp. 445.

[31] Deng, X. and Tian, X. (2011), "A new fault isolation method based on unified contribution plots", *Proceedings of the 30th Chinese Control Conference, CCC 2011,* pp. 4280.

[32] Liu, J. and Chen, D. -. (2012), "Multiple Sensor Fault Isolation Using Contribution Plots without Smearing Effect to Non-Faulty Variables", *Computer Aided Chemical Engineering,* vol. 31, pp. 1517-1521.

[33] Mnassri, B., El Adel, E. M., Ananou, B. and Ouladsine, M. (2009), "Fault detection and diagnosis based on PCA and a new contribution plots", *IFAC Proceedings Volumes (IFAC-PapersOnline),* pp. 834.

[34] Ramírez, A. W. and Llinàs, J. C. (2011), "Fault diagnosis of batch processes release using PCA contribution plots as fault signatures", *ICEIS 2011 - Proceedings of the 13th International Conference on Enterprise Information Systems,* Vol. 1 DISI, pp. 223.

[35] Pennacchi, P. and Vania, A. (2008), "Diagnostics of a crack in a load coupling of a gas turbine using the machine model and the analysis of the shaft vibrations", *Mechanical Systems and Signal Processing,* vol. 22, no. 5, pp. 1157-1178.

[36] Ahmed, M., Baqqar, M., Gu, F. and Ball, A. D. (2012), "Fault detection and diagnosis using Principal Component Analysis of vibration data from a reciprocating compressor", *Proceedings of the 2012 UKACC International Conference on Control, CONTROL 2012,* pp. 461.

[37] Cui, L., Wang, J. and Lee, S. (2014), "Matching pursuit of an adaptive impulse dictionary for bearing fault diagnosis", *Journal of Sound and Vibration,* vol. 333, no. 10, pp. 2840-2862.

[38] Sekhar, A. S. and Prabhu, B. S. (1995), "Effects of coupling misalignment on vibrations of rotating machinery", *Journal of Sound and Vibration,* vol. 185, no. 4, pp. 655-671.

[39] Patel, T. H. and Darpe, A. K. (2009), "Vibration response of misaligned rotors", *Journal of Sound and Vibration,* vol. 325, no. 3, pp. 609-628.

[40] Avendano, R. D. and Childs, D. W. (2013), "One explanation for two-times running speed response due to misalignment in rotors connected by flexible couplings", *Journal of Engineering for Gas Turbines and Power,* vol. 135, no. 6.

[41] Saavedra, P. N. and Ramírez, D. E. (2004), "Vibration analysis of rotors for the identification of shaft misalignment part 1: Theoretical analysis", *Proceedings of the Institution of Mechanical Engineers, Part C: Journal of Mechanical Engineering Science,* vol. 218, no. 9, pp. 971-985.

[42] Saavedra, P. N. and Ramírez, D. E. (2004), "Vibration analysis of rotors for the identification of shaft misalignment part 2: Experimental validation", *Proceedings of the Institution of Mechanical Engineers, Part C: Journal of Mechanical Engineering Science,* vol. 218, no. 9, pp. 987-999.

[43] Gibbons, C. B. (1976), "Coupling missalignment forces", *Proceedings of the 5th Turbomach Symposium,* October 1976, Texas, USA, pp. 111.

[44] Peng, Z. K., Chu, F. L. and Tse, P. W. (2007), "Singularity analysis of the vibration signals by means of wavelet modulus maximal method", *Mechanical Systems and Signal Processing,* vol. 21, no. 2, pp. 780-794.

[45] Sekhar, A. S. (2005), "Identification of unbalance and crack acting simultaneously in a rotor system: Modal expansion versus reduced basis dynamic expansion", *JVC/Journal of Vibration and Control,* vol. 11, no. 9, pp. 1125-1145.

[46] Negiz, A. and Çinar, A. (1998), "Monitoring of multivariable dynamic processes and sensor auditing", *Journal of Process Control,* vol. 8, no. 5-6, pp. 375-380.